PNAS RESEARCH ARTICLE | MEDICAL SCIENCES

DARPins as pan-reactivators of temperature-sensitive p53 cancer mutants

Philipp Münick[a,1], Dimitrios-Ilias Balourdas[b,c,1], Julianne S. Funk[d], Büşra Yüksel[a,e], Danai Mavridi[b,c], Justin Heftel[a,e], Birgit Dreier[f], Jonas V. Schaefer[f], Birgit Schäfer[a], Stefan Knapp[b,c], Tümay Telatar[g], Baki Akgül[g], Andreas Plückthun[f], Thorsten Stiewe[d,h,i], Andreas C. Joerger[b,c,2], and Volker Dötsch[a,2]

Affiliations are included on p. 10.

Edited by Carol Prives, Columbia University, New York, NY; received November 12, 2025; accepted March 27, 2026

The tumor suppressor p53 is the most frequently mutated protein in tumors and a target for drug development. More than 2000 cancer-associated p53 missense mutations have been reported, most of them located in the DNA-binding domain (DBD). Due to the low intrinsic thermostability of the latter, they often lead to unfolding at physiological temperature. Stabilizing the DBD with small molecules has been shown to be effective in reactivating the cavity-creating cancer mutant Y220C. Unfortunately, the majority of p53 mutants seem to lack druggable binding pockets for small molecules. Here we show that a designed ankyrin repeat protein (DARPin) that binds to the p53 DBD stabilizes temperature-sensitive (TS) p53 cancer mutants, thereby compensating for mutation-induced loss of stability. We determined high-resolution crystal structures of multiple DARPin–mutant p53 complexes, providing mechanistic insights into this mode of stabilization. Reporter gene assays across a comprehensive panel of cancer-associated mutants revealed reactivation of the majority of TS mutants, whereas DNA-contact mutants and those with local misfolding of the DNA-binding surface remained inactive, as expected. We demonstrate that this reactivation induces the transcription of canonical p53 target genes and elicits antiproliferative effects in cancer cell lines. A combination of this DARPin with an mRNA/lipid nanoparticle-based transfection approach may have the potential to reactivate most TS p53 mutants and resensitize cancer cells to chemotherapy.

p53 | cancer | DARPin | mutation | reactivation

Significance

The tumor suppressor p53, a central guardian against malignant transformation, is inactivated by mutation in about half of all human cancers. Many p53 mutants are temperature-sensitive (TS), exhibiting reduced conformational stability yet retaining the potential for reactivation by stabilizing agents. However, the absence of suitable drug-binding pockets has limited the development of such molecules. Here, we introduce designed ankyrin repeat proteins (DARPins) as generic mutant p53 stabilizers that bind a nonfunctional site on the p53 DNA-binding domain. This interaction compensates for mutation-induced loss of thermal stability and restores p53 signaling in patient-derived cancer cells. Coupled with mRNA-based delivery, this approach could enable broad-spectrum reactivation of TS mutants for personalized cancer therapy.

The transcription factor p53, arguably the most important tumor suppressor, is inactivated by mutations in about 50% of cancers, making the reactivation of mutant p53 a potential therapeutic strategy for cancer (1–3). Most oncogenic p53 mutations are missense mutations mapping to its DNA-binding domain (DBD) (4). More than 2000 different missense-variants have been identified in tumors, and, apart from the hotspot mutants, most of them are only poorly characterized (5–7). Mechanistically, the mutations can be divided into two classes: (i) DNA-contact mutations that remove an essential DNA-contact, which prevents p53 from binding to its target promoters, and (ii) structural mutations that lower the thermostability of the intrinsically unstable p53 protein to varying degrees, causing it to unfold and aggregate under physiological conditions (8, 9). A subset of those structural mutants is particularly attractive from a drug discovery perspective as they are temperature-sensitive (TS). They exhibit a loss of function under physiological conditions but retain at least some degree of transcriptional activity at low (permissive) temperatures, where they are correctly folded and adopt a wild-type-like conformation (5, 8, 10–12). An estimated 15-25% of cancer-associated p53 mutants may belong to this category (11, 13), making them promising candidates for pharmacological reactivation.

p53 has long been considered undruggable. The destabilizing, cavity-creating p53 cancer hotspot mutation Y220C, however, is an excellent paradigm for the development of drugs based on protein stabilization (14–16). Several classes of small molecules have been identified that bind to a mutation-induced pocket on the surface of the Y220C mutant (and the related Y220S/N mutants), thereby increasing its thermostability and slowing its aggregation (15–22). Importantly, some of these small-molecule stabilizers are biologically active in cancer cells with a homozygous Y220C mutation and restore p53 signaling (19, 20, 23, 24), providing proof of concept that pharmacological rescue of TS cancer mutants with chemical chaperones is a promising strategy. The Y220C reactivator rezatapopt, developed by PMV Pharmaceuticals, is currently in phase I/II clinical trials, with encouraging results (25, 26).

Competing interest statement: Andreas Plückthun is a co-founder and shareholder of Molecular Partners AG, who are commercializing the DARPin technology. The other authors declare no competing interests. A patent application for "Designed ankyrin repeat proteins binding p53, and uses thereof" has been filed (WO2026013280A1).

This article is a PNAS Direct Submission.

Copyright © 2026 the Author(s). Published by PNAS. This article is distributed under Creative Commons Attribution-NonCommercial-NoDerivatives License 4.0 (CC BY-NC-ND).

[1]P.M. and D.-I.B. contributed equally to this work.

[2]To whom correspondence may be addressed. Email: Joerger@pharmchem.uni-frankfurt.de or vdoetsch@em.uni-frankfurt.de.

This article contains supporting information online at https://www.pnas.org/lookup/suppl/doi:10.1073/pnas.2531747123/-/DCSupplemental.

Published April 28, 2026.

Downloaded from https://www.pnas.org by UNIVERSITAET ZUERICH; HAUPTBIBLIOTHEK NATURWISSENSCHAFTEN on April 29, 2026 from IP address 130.60.168.8.

However, only a fraction of p53 cancer mutants have targetable cavities, and, ideally, one would like to identify broadly acting mutant p53 stabilizers to cover a wider spectrum of destabilizing mutations. Toward this goal, recent studies have shown that many—though not all—structural p53 mutants can be reactivated by arsenic trioxide (ATO), which stabilizes the DBD by covalently binding to three cysteines (Cys124, Cys135, Cys141) within a cryptic binding site in the loop-sheet-helix motif (27, 28). A follow-up study demonstrated similar effects for the antiparasitic drug potassium antimony tartrate, in which the antimony atom binds noncovalently to the same cryptic allosteric site as ATO but rescues a much smaller subset of mutants overall (29). However, the widespread therapeutic use of these compounds is somewhat limited by their general toxicity and their lack of specificity.

Biologics may have the potential to stabilize a broader set of p53 mutants, thereby rescuing the activity of this critical tumor suppressor. Recently, we developed a designed ankyrin repeat protein (DARPin) that binds to the DBD of p53 without interfering with DNA binding (30). This binding site overlaps with the binding site of the human papillomavirus (HPV) E6 protein that mediates p53 degradation in infected cells (31–33). We have demonstrated that the delivery of the DARPin into cells via mRNA-containing lipid nanoparticles (LNPs) prevents this degradation, thereby restoring p53 protein levels and initiating a p53-dependent transcriptional program (30). Here, we show that this DARPin also stabilizes many TS p53 cancer mutants and reactivates p53-mediated cell-cycle arrest, suggesting its potential therapeutic use as a potent pan-TS p53 mutant reactivator.

Results

DARPin C10-H82R as a Generic Reactivator of Temperature-Sensitive p53 Cancer Mutants. DARPins are ideally suited for intracellular applications as stabilizers or inhibitors (34, 35). They are small (14-18 kDa), thermodynamically highly stable, and lack disulfide bridges, which would otherwise limit their applicability under the reducing conditions in the cytoplasm. Recently, we developed DARPins as binding modules for all folded domains of p63 and p73, which can be used for detection and for intracellular inhibition (36, 37)—or covalently linked to E3 ligases as bioPROTACS for selective protein degradation (38). Additionally, we developed a DARPin (DARPin C10 and a rationally engineered higher-affinity variant, C10-H82R) that binds to the DBD of p53 without inhibiting its DNA-binding activity, but instead blocks interaction with the HPV E6 protein, thereby preventing HPV-mediated p53 degradation (30). Any molecule that binds to the folded, but not the unfolded, state of a protein should shift the equilibrium toward the folded state and thereby stabilize it. We, therefore, speculated that DARPin C10-H82R could potentially also stabilize the DBD of conformationally unstable p53 cancer mutants, providing an additional therapeutic application.

To test this hypothesis, we first analyzed the interaction between the DARPin and selected p53 mutants using isothermal titration calorimetry (ITC) at 20 °C. The selected TS mutants were predicted to adopt a wild-type-like conformation at this temperature, and, consistent with this prediction, all mutants bound the DARPin with a K_d ranging from 37 to 103 nM, similar to the K_d for the wild-type p53 DBD (33 nM) (Table 1 and Fig. 1 *A–D* and *SI Appendix*, Fig. S1).

We next investigated the potential stabilizing effect of binding by determining the melting temperature, T_m, of the selected p53 mutant DBDs with and without DARPin C10-H82R by differential scanning fluorimetry (DSF). The panel of mutants included both moderately destabilized mutants such as R158L (ΔT_m = −5.7 °C, relative to the wild type) and severely destabilized mutants such as E285K (ΔT_m = −11.8 °C). As shown in Fig. 1*E*, DARPin C10-H82R stabilized all p53 mutant DBDs in a concentration-dependent manner, with melting temperature increases of up to 10 °C, thereby in most cases compensating for the mutation-induced stability loss and restoring a wild-type-like thermal stability. These results suggest that DARPin binding can sufficiently stabilize most TS p53 cancer mutants to induce at least partial functional reactivation in cancer cells.

Table 1. Thermodynamic parameters of DARPin C10-H82R binding to different p53 DBD variants determined by ITC

p53 DBD variant	K_d (nM)*	ΔH (kcal/mol)	ΔS (cal/mol·K)	Replicates
WT	32.6 ± 6.2	−18.4 ± 0.4	−28.6 ± 1.4	4
V157F	102.5 ± 15.7	−18.1 ± 0.2	−29.6 ± 0.8	3
R158L	37.1 ± 9.1	−19.3 ± 0.4	−31.7 ± 2.0	3
Y220C	60.6 ± 28.8	−19.8 ± 0.9	−34.2 ± 2.0	3
Y234C	45.8 ± 2.6	−18.2 ± 0.2	−28.4 ± 0.9	3
V272M	41.1 ± 5.5	−18.0 ± 0.1	−27.8 ± 0.7	2
R282W	61.2 ± 19.7	−19.6 ± 0.5	−33.6 ± 2.4	3
E285K	48.8 ± 3.7	−19.5 ± 0.2	−33.1 ± 0.8	3

*Mean ± SD, measured at 20 °C.

Structures of DARPin-Mutant p53 Complexes. To confirm that DARPin binding stabilizes a wild-type-like conformation of p53 mutants, we determined high-resolution crystal structures of DARPin C10 with the DBD of p53 cancer mutants V143A, V157F, Y220C, Y234C, V272M, and R282W, as well as of DARPin C10-H82R with mutant E285K (Fig. 2 and *SI Appendix*, Tables S1 and S2). These structures confirmed the mutation-induced structural changes in the p53 DBD seen for the isolated DBD mutants (14, 39, 40) and further revealed distinct mechanisms of destabilization: creation of internal cavities for the large-to-small substitutions V143A and Y234C, creation of an extended surface crevice in Y220C, expansion of the hydrophobic core for the small-to-large substitution V157F, distortions in the loop-sheet-helix motif in R282W, loss of the Lys132-Glu285 salt bridge in E285K, and structural rearrangements in the hydrophobic core around residue 272, including the adjacent cysteine cluster, in V272M (*SI Appendix*, Fig. S2).

The overall p53–DARPin interface was conserved for most mutants, with some fluidity of the interface in the V157F mutant complex (Fig. 2 *A* and *B*). The strong conservation of the interface area is consistent with the comparable dissociation constants measured by ITC (Table 1). As for the wild-type p53 DBD, the interface with the mutants is characterized by a central hydrophobic cluster of three tryptophan side chains (p53-Trp146, C10-Trp13, and C10-Trp46) surrounded by salt-bridge networks involving p53 residues Arg110 and Asp148. In the DARPin C10-H82R complex with mutant E285K, this salt-bridge network is further extended by an additional salt-bridge between Arg82 and Asp228 in the p53 DBD, as seen for the corresponding complex with the wild-type DBD (PDB entry 9FZB).

In the complex with R282W, the mutation site is in close proximity to the DARPin interface, causing a reorientation of the L1 loop in which the His115 side chain no longer interacts with the DARPin backbone (Fig. 2*C*). In addition, the complex of DARPin C10 with the V157F mutant displayed notable structural plasticity, with the interface being shifted slightly. The small-to-large mutation V157F induces steric strain in the hydrophobic core of the DBD, resulting in a shift of the adjacent Tyr220 side chain

Downloaded from https://www.pnas.org by UNIVERSITAET ZUERICH; HAUPTBIBLIOTHEK NATURWISSENSCHAFTEN on April 29, 2026 from IP address 130.60.168.8.

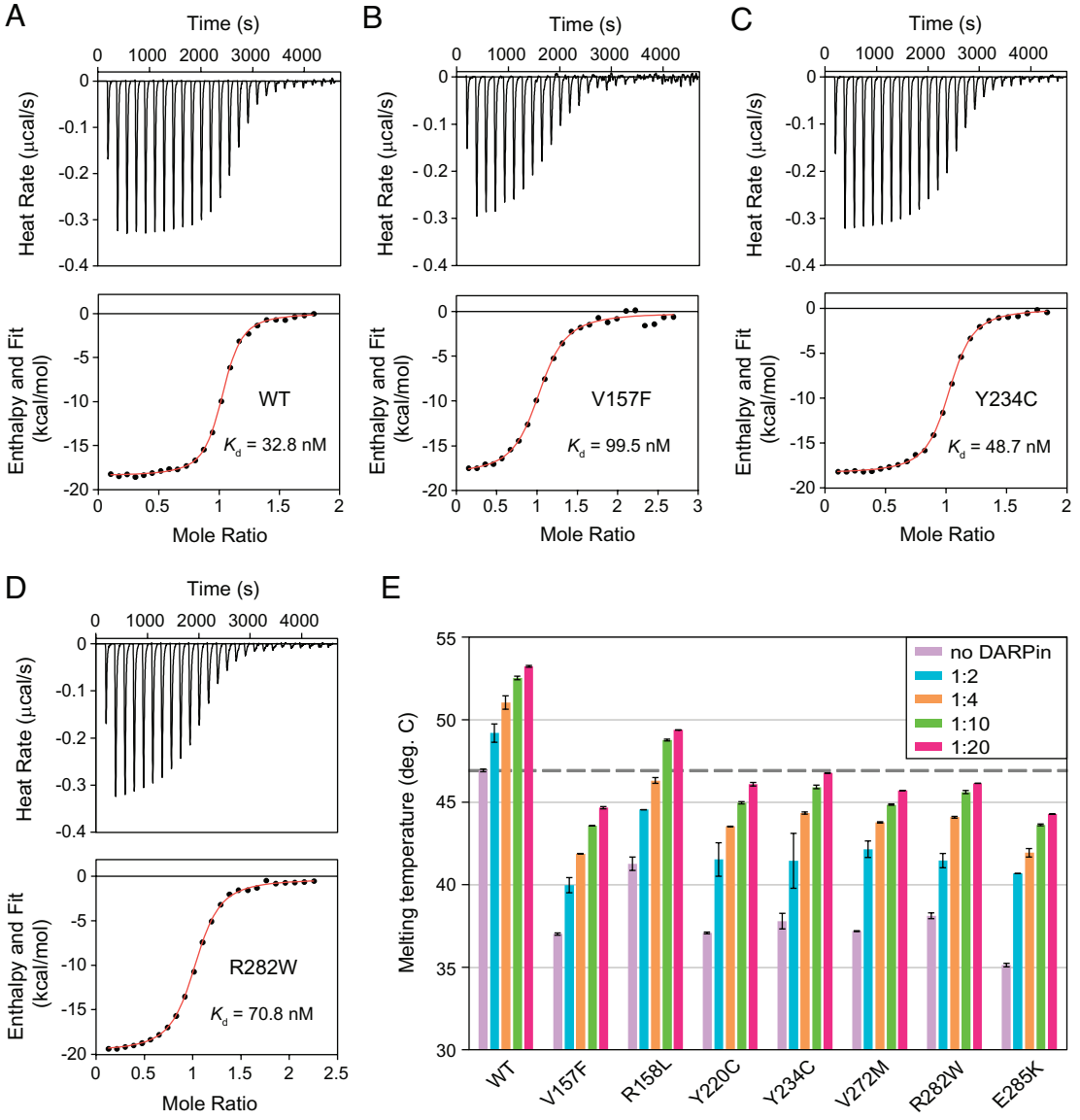

Fig. 1. Affinity and stability effects of DARPin C10-H82R on the DBD of p53 cancer mutants. (*A*–*D*) Representative ITC curves and derived dissociation constants (K_ds) of the complexes of DARPin C10-H82R with different p53 DBD variants, measured at 20 °C; see also Table 1. (*A*) Wild-type p53. (*B*) V157F mutant. (*C*) Y234C mutant. (*D*) R282W mutant. (*E*) Melting temperatures (T_m) of p53 cancer mutants in their unbound state and with increasing concentration of DARPin C10-H82R, measured by DSF. The dashed line indicates the melting temperature of the native wild-type p53 DBD, showing that most mutant DBDs regain a wild-type-like stability at high DARPin concentrations.

and rearrangement of the S7/S8 loop at the periphery of the DARPin interface (Fig. 2*B*). This repositioning allows Asp228 in the S7/S8 loop to interact with the DARPin directly, forming a salt bridge with Arg79 and a hydrogen bond with the indole nitrogen of Trp46. These mutant-specific changes at the periphery of the p53–DARPin interface may provide opportunities for further DARPin optimization for these two mutants.

DARPins Reactivate Temperature-Sensitive Structural p53 Cancer Mutants in Transiently Transfected Cells. To systematically assess the effects of our DARPins on the p53 activity in cells, we performed reporter gene assays with the pBDS-2 promoter in H1299 cells transiently cotransfected with plasmids expressing a specific p53 mutant together with either a control DARPin, DARPin C10, or the optimized variant C10-H82R. We tested all TS mutants represented among the top 40 missense variants of the IARC/NCI and UMD *TP53* mutation database (41, 42), as well as a set of additional low-frequency TS mutants. We also included mutant classes that cannot be reactivated by simple thermodynamic stabilization of the DBD as a control (Fig. 3*A*). As expected, DNA-contact mutants (R248W and R273H) and mutants with local perturbation in the DNA-binding surface, such as G245S, R249S, and Y163C, were not reactivated. Similarly, the mutants R175H and H179Y, which are deficient in zinc binding, could not be rescued either. In contrast, almost all cancer mutants in our panel with a reported TS phenotype (11, 43–46) showed at least some degree of reactivation, with C10-H82R consistently achieving stronger transactivation than the parental DARPin C10. For some mutants, such as R158H, up to 70% of the wild-type activity of p53 could be restored. The degree of reactivation correlated with the mutation-induced stability loss at a particular residue. For example, V157L showed a higher reactivation level than V157F, and Y220H a higher reactivation level than Y220C. In both cases, the more strongly reactivated mutant is less destabilized by the mutation (16, 46). Another interesting mutant pair was H193Y and H193R: the tyrosine variant was

Downloaded from https://www.pnas.org by UNIVERSITAET ZUERICH; HAUPTBIBLIOTHEK NATURWISSENSCHAFTEN on April 29, 2026 from IP address 130.60.168.8.

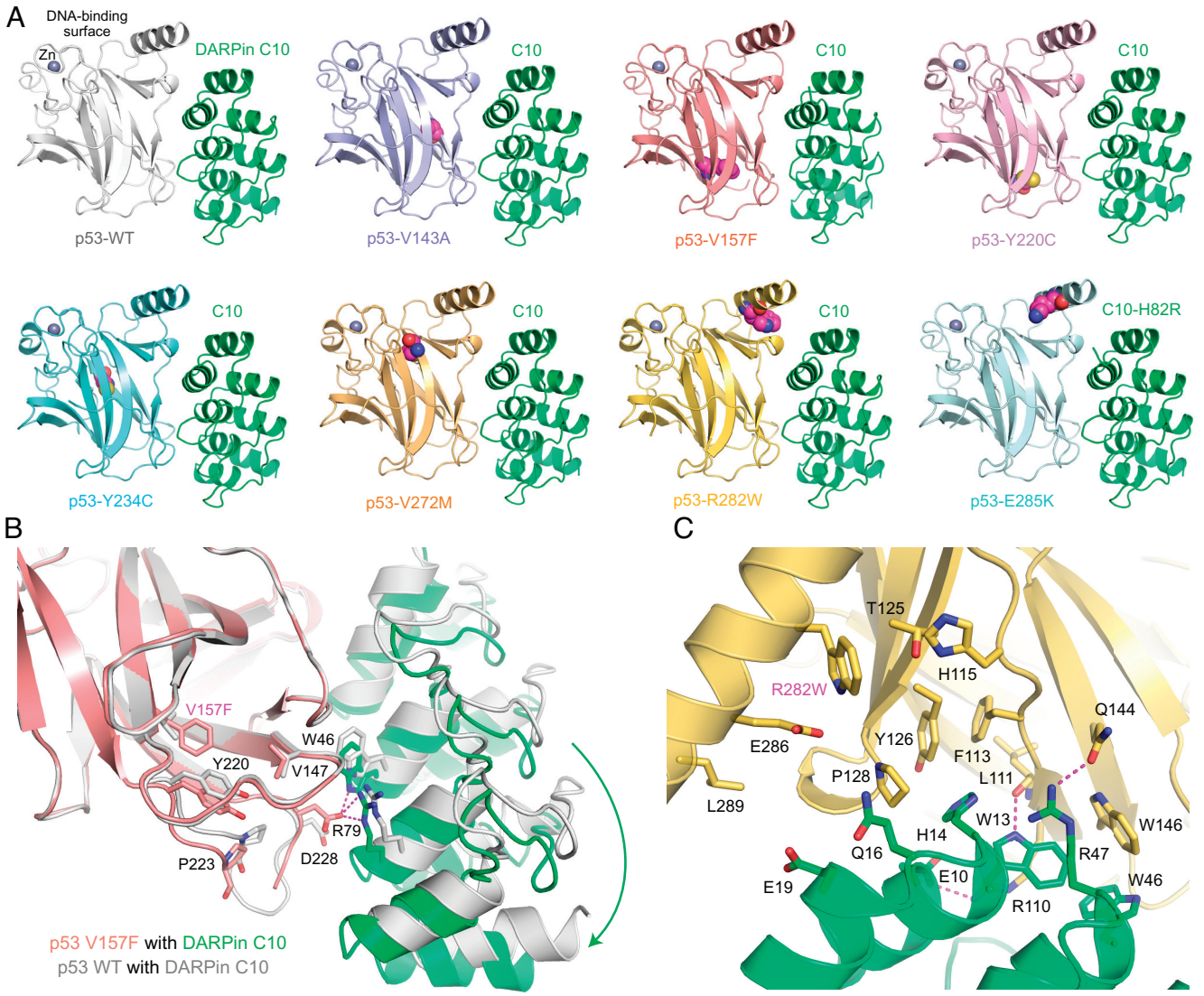

Fig. 2. Structures of p53 cancer mutant DBDs bound to DARPin C10. (*A*) Overall structures of the complexes of the p53 wild-type DBD and mutants V143A, V157F, Y220C, Y234C, V272M, R282W, and E285K with DARPin C10 or DARPin C10-H82R. The mutation sites in p53 are shown as magenta sphere models. (*B*) Superimposition of the wild-type (gray cartoon) and V157F mutant DARPin complex (salmon and green cartoon models), highlighting the mutation-induced shift in the p53–DARPin interface. (*C*) Close-up view of the periphery of the R282W–DARPin interface around the mutation site and the L1 loop. The p53 DBD is shown in yellow, DARPin C10 in green. Selected residues are shown as stick models, and polar interactions are highlighted with dashed lines.

successfully reactivated, whereas the arginine variant showed no reactivation, indicating that introduction of an arginine in the L3-loop region packing against the edge of the β-sandwich resulted in severe local misfolding. The few potential TS mutants that did not show a significant reactivation, i.e. Y205C and Y236C, were cases of particularly unstable mutants where the apparent melting temperature of the DBD is reduced by 14 and 17 °C, respectively (40). The same pattern of reactivation was observed in reporter gene assays with the p21 promoter, with reactivation levels for individual mutants being generally higher than those observed with the synthetic promoter (Fig. 3*B*).

In summary, DARPin C10-H82R reactivated almost all tested p53 TS mutants, restoring up to 85% of wild-type activity, with reactivation levels correlating with the degree of mutation-induced destabilization.

Reactivation in CRISPR Knock-In p53 Mutant Cell Lines. We next evaluated the ability of DARPins to reactivate mutant p53 expressed from the endogenous *TP53* locus in cancer cells. To this end, we employed a panel of recently generated CRISPR-engineered HCT116 cell lines carrying mutations in the endogenous *TP53* gene (46). This panel included four TS mutants: R158H, which had shown the best response in the reporter genes assay, the classical TS mutant V272M (47), and two TS mutants that we had recently identified (V157L and T256A) (46). The DNA-contact mutant R273H was included as a negative control. In addition to the DARPin, we treated cells with the MDM2 inhibitor Nutlin-3a (N3a). This inhibitor blocks the interaction of MDM2 with the transactivation domain of p53 and prevents the ubiquitination-based degradation of p53, thus increasing cellular p53 protein levels (48, 49). Upon transfection of DARPin C10-H82R mRNA in combination with N3a treatment, we observed induction of the p53 target gene *CDKN1A*/*p21* in all four TS mutants tested (Fig. 4*A*). Expectedly, the R273H control did not induce *p21* expression in response to DARPin C10-H82R, confirming that only TS mutants are reactivated. Among these, T256A displayed the most robust reactivation. We therefore further engineered T256A cells by transduction of a doxycycline (Dox)-inducible DARPin expression construct (pInd_cDP or pInd_C10-H82R). Induction of DARPin C10-H82R in the presence of N3a led

Downloaded from https://www.pnas.org by UNIVERSITAET ZUERICH; HAUPTBIBLIOTHEK NATURWISSENSCHAFTEN on April 29, 2026 from IP address 130.60.168.8.

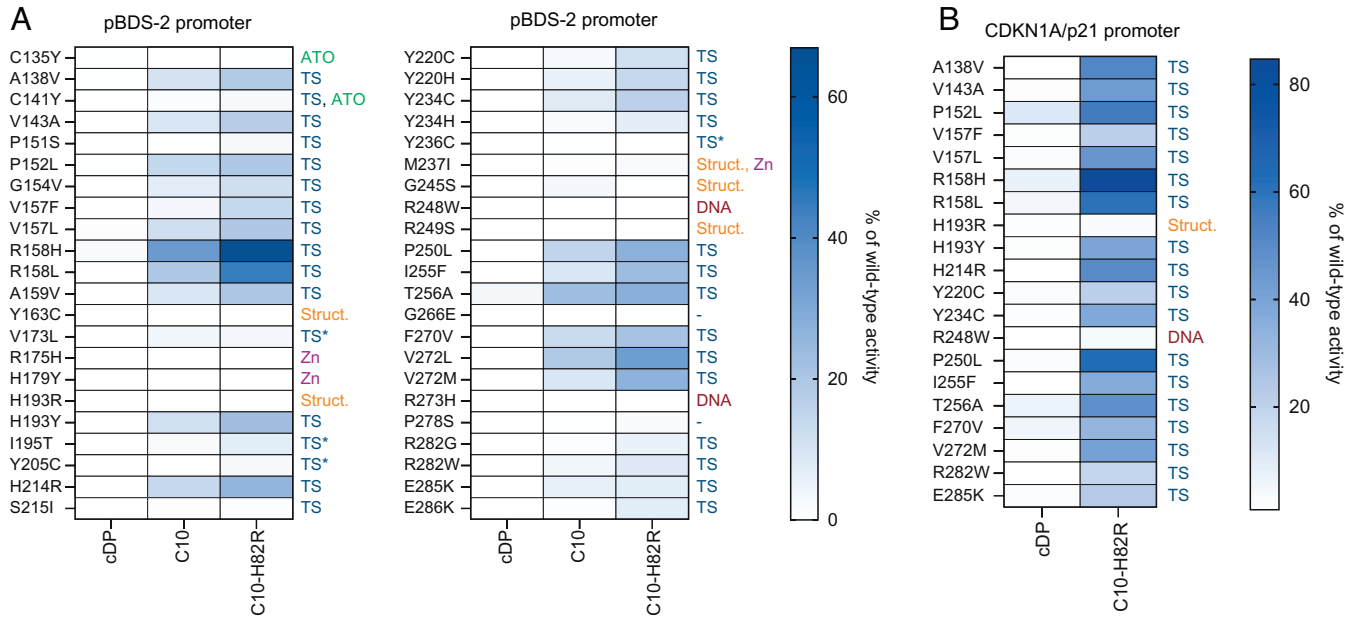

Fig. 3. Transactivation assays in H1299 cells (p53$^{-/-}$) using luciferase reporters driven by the synthetic pBDS-2 promoter (*A*) or the CDKN1A/p21 (*B*) promoter to assess reactivation of p53 mutants by DARPin C10 or DARPin C10-H82R. Transcriptional activity is shown relative to H1299 cells transfected with wild-type p53. The classification of each mutant is indicated on the *right* side of the heatmap: TS = temperature-sensitive mutant; Struct. = structural mutant with local distortion in the L3-loop region; Zn = zinc-binding-deficient mutant, DNA = DNA-contact mutant, ATO = cysteines targeted by arsenic trioxide. Mutants were classified as TS based on either an experimentally determined TS phenotype in at least one of the following references (10–12, 44–46) or structural considerations based on available crystal structures (TS*). The heatmap represents the mean value of three biological replicates, the raw data for each replicate are provided in Datasets S1 and S2.

to strong p21 upregulation (Fig. 4*B*) and a marked reduction of cells in S-phase, consistent with a p53-mediated cell-cycle arrest (Fig. 4*C* and *SI Appendix*, Fig. S3). Notably, DARPin expression was restricted to ~30 to 40% of cells after Dox induction, suggesting that the effects observed in Western blots (Fig. 4*B*) may underestimate the full reactivation potential in mutant cell lines.

Restoration of p53 Target Gene Expression and Induction of Cell-Cycle Arrest in Patient-Derived Cancer Cell Lines. Variants with mutation at residue Arg158 showed strong reactivation by DARPin C10-H82R in our assays. In addition, variants with mutations at positions Val157 or Ala159 also responded well to expression of the DARPins. Notably, substitutions at these three residues are particularly common in lung cancer due to a specific mutagenesis mechanism triggered by benzopyrenes in cigarette smoke (50–52). Next, we tested whether the high levels of reactivation observed in the transactivation assays using transiently transfected cells could be confirmed in patient-derived cell lines expressing mutant p53 from the endogenous locus. To this end, the lung cancer cell lines NCI-H441 (R158L) and NCI-H2087 (V157F), the liver cancer cell line Huh7 (Y220C) as well as the vulvar squamous cell carcinoma cell line SW954 (R158H) were transfected with the mRNA encoding either DARPin C10-H82R or the control DARPin. Cells were harvested 24 h after transfection, and the mRNA level of the p53 target genes *PUMA*, *NOXA*, *p21,* and *MDM2* was determined by reverse transcription quantitative PCR (RT qPCR). These data showed that in all four cell lines, expression of DARPin C10-H82R led to a robust upregulation of *PUMA*, *p21*, and *MDM2*, which was particularly pronounced for the Y220C mutant, whereas *NOXA* levels were only moderately elevated relative to the control DARPin (Fig. 5 *A–D*). Caspase-Glo 3/7 assays showed a small increase in the activity of caspases 3 and 7 in all four cell lines following expression of DARPin C10-H82R (*SI Appendix*, Fig. S4).

Elevated levels of MDM2 protein would, however, also lead to faster degradation of the reactivated p53. We therefore investigated whether higher reactivation levels could be achieved by adding the MDM2 inhibitor N3a in addition to transfection with the DARPin C10-H82R. Indeed, inhibition of MDM2 resulted in a higher transcriptional activity of the stabilized p53 (Fig. 5 *A–D*). This effect was not observed in cells transfected with the control DARPin, indicating that the enhanced transcriptional activity of p53 in DARPin/N3a-treated cells requires both thermal stabilization and prolonged half-life of the reactivated protein.

We next assessed the effects of the DARPin on cell-cycle progression in SW954 and NCI-H411 cells, which harbor the two mutations (R158H/L) that exhibited the highest reactivation levels across all assays. Target gene transactivation following C10-H82R expression induced cell-cycle arrest. The strongest reduction in S-phase cells was observed in SW954, and in both cell lines this effect was further enhanced by N3a (Fig. 5*E*). In addition, long-term colony formation assays demonstrated that C10-H82R reduces clonogenic growth in both cell lines, again with a markedly more pronounced effect observed in SW954 (Fig. 5*F*).

Altogether, the data from the patient-derived cell lines show that a key biological effect of DARPin C10-H82R is the slowdown of proliferation, consistent with studies on reactivation of the Y220C mutant using the small-molecule stabilizer rezatapopt, in which growth inhibition and cell-cycle effects were also prominent outcomes (25, 26, 53).

DARPin C10-H82R Does Not Induce Upregulation of p53 Target Genes in Primary Human Fibroblasts. The experiments described above demonstrate that the DARPins can be used to stabilize TS p53 mutants and restore a p53-dependent transcriptional program in cancer cells. In combination with an mRNA/LNP-based approach for the transfection of cells, these DARPins may therefore have a promising therapeutic potential for cancer therapy. However, the DARPins also increased the

Downloaded from https://www.pnas.org by UNIVERSITAET ZUERICH; HAUPTBIBLIOTHEK NATURWISSENSCHAFTEN on April 29, 2026 from IP address 130.60.168.8.

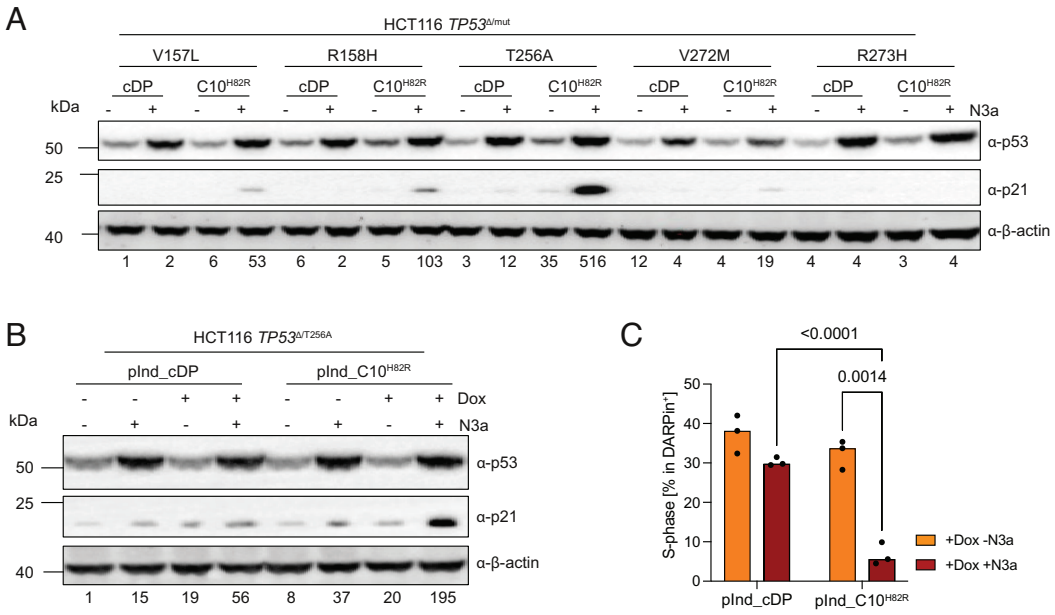

Fig. 4. DARPin-induced reactivation of mutant p53 in CRISPR-engineered cell lines. (*A*) Immunoblot following mRNA delivery of the indicated DARPins combined with Nutlin-3a (N3a)-mediated stabilization of mutant p53. Numbers indicate p21 band intensity normalized to β-actin. (*B*) Immunoblot of HCT116 *TP53*$^{\Delta/T256A}$ cells transduced with a doxycycline (Dox)-inducible DARPin expression vector (pInd_cDP or pInd_C10^{H82R}), in the presence or absence of N3a. Numbers indicate p21 band intensity normalized to β-actin. (*C*) Fraction of DARPin-expressing HCT116 *TP53*$^{\Delta/T256A}$ cells in S-phase, analyzed by parallel DARPin and EdU staining (*SI Appendix*, Fig. S3). Median of three biological replicates. Statistical significance was assessed using two-way ANOVA, p-values are shown. Dox, doxycycline; N3a, Nutlin-3a.

thermal stability of wild-type p53, and such a stabilization could result in the upregulation of a p53-based transcriptional program in noncancerous cells as well. In an earlier study, we investigated the effect of DARPin C10 in U2-OS cells, a cancer cell line harboring wild-type p53 (30). RNAseq experiments revealed only a small number of differentially regulated genes, most of which were not p53 target genes. To further investigate the effect of our DARPins in noncancerous cells, we transfected primary human fibroblasts with the mRNA of DARPin C10-H82R. Staining of these cells with the anti-p53 antibody DO-I showed no increase in the cellular level of p53 relative to no DARPin or a control DARPin (Fig. 6 *A* and *B*). Using RT-qPCR for probing the mRNA levels of p53 target genes showed no significant increase for *PUMA*, *NOXA*, *p21,* or *MDM2* Fig. 6 *C–F*). Importantly, addition of N3a to the DARPin-treated cells resulted in a significant upregulation of *PUMA*, *p21,* and *MDM2* (*SI Appendix*, Fig. S5), as expected, indicating that DARPin binding does not disrupt the critical MDM2 negative feedback loop. These results suggest that DARPin treatment does not activate wild-type p53 and is unlikely to be associated with p53-related toxicity in nontumorigenic cells.

Discussion

The tumor suppressor p53 has been the focus of many drug development projects aimed at restoring a p53-dependent program in cancer cells, leading to cell-cycle arrest or apoptosis. While the reactivation of DNA-contact mutants such as R248W remains challenging, if possible at all, the use of small organic molecules that bind to mutation-induced pockets in the DBD to stabilize and reactivate conformationally unstable mutants has been proven successful in the case of the Y220C and Y220S mutants (25, 26, 53). Unfortunately, only a small fraction of the mutations in the p53 DBD create druggable binding pockets accessible to small molecules. In contrast, small binding proteins represent an attractive alternative: they can bind to larger surfaces and, crucially, do not depend on binding pockets, and thus have the potential to stabilize a large set of conformationally unstable mutants. We recently described a DARPin that binds to the p53 DBD without affecting DNA binding and blocks interaction with the HPV E6 protein, thus protecting wild-type p53 from HPV-mediated degradation (30).

Here, we demonstrated that the same DARPin also increases the thermodynamic stability of the p53 DBD and strongly stabilizes TS p53 cancer mutants, offering an exciting alternative therapeutic strategy as a generic mutant p53 reactivator. All tested mutants with a reported TS phenotype showed at least some degree of reactivation upon treatment with our DARPin, with reactivation levels correlating, to some extent, with the degree of mutation-induced destabilization (Fig. 3). Moderately destabilized mutants showed stronger reactivation levels than severely destabilized variants at a given DARPin concentration. The V157L and T256A mutants reactivated in our reporter gene assay belong to a special subset of mutants (collectively covering about 20% of the p53 missense mutations) that were classified as benign in cDNA-based screens but as loss-of-function mutations in our recent systematic mutational scan of the p53 DBD at endogenous protein levels (46). We had shown that many of these mutants are only moderately destabilized, suggesting that they represent promising targets for pharmacological reactivation. Many mutants of this subgroup may therefore be particularly responsive to DARPin-based therapy.

More than 2,000 different p53 missense mutations have been reported in human tumors, making the development of personalized medicines challenging. Most individual mutations are relatively rare, rendering the development of mutation-selective therapy economically unfeasible in most cases. Our DARPin-based approach instead offers a broad-spectrum therapeutic strategy capable of reactivating many, if not most, TS p53 cancer mutants. An estimated 15 to 25% of the p53 cancer mutome are TS mutations that should, in principle, be amenable to DARPin-based reactivation. This corresponds to 1.5 to 2.5 million new cancer cases per year worldwide, based on a global cancer incidence of

Downloaded from https://www.pnas.org by UNIVERSITAET ZUERICH; HAUPTBIBLIOTHEK NATURWISSENSCHAFTEN on April 29, 2026 from IP address 130.60.168.8.

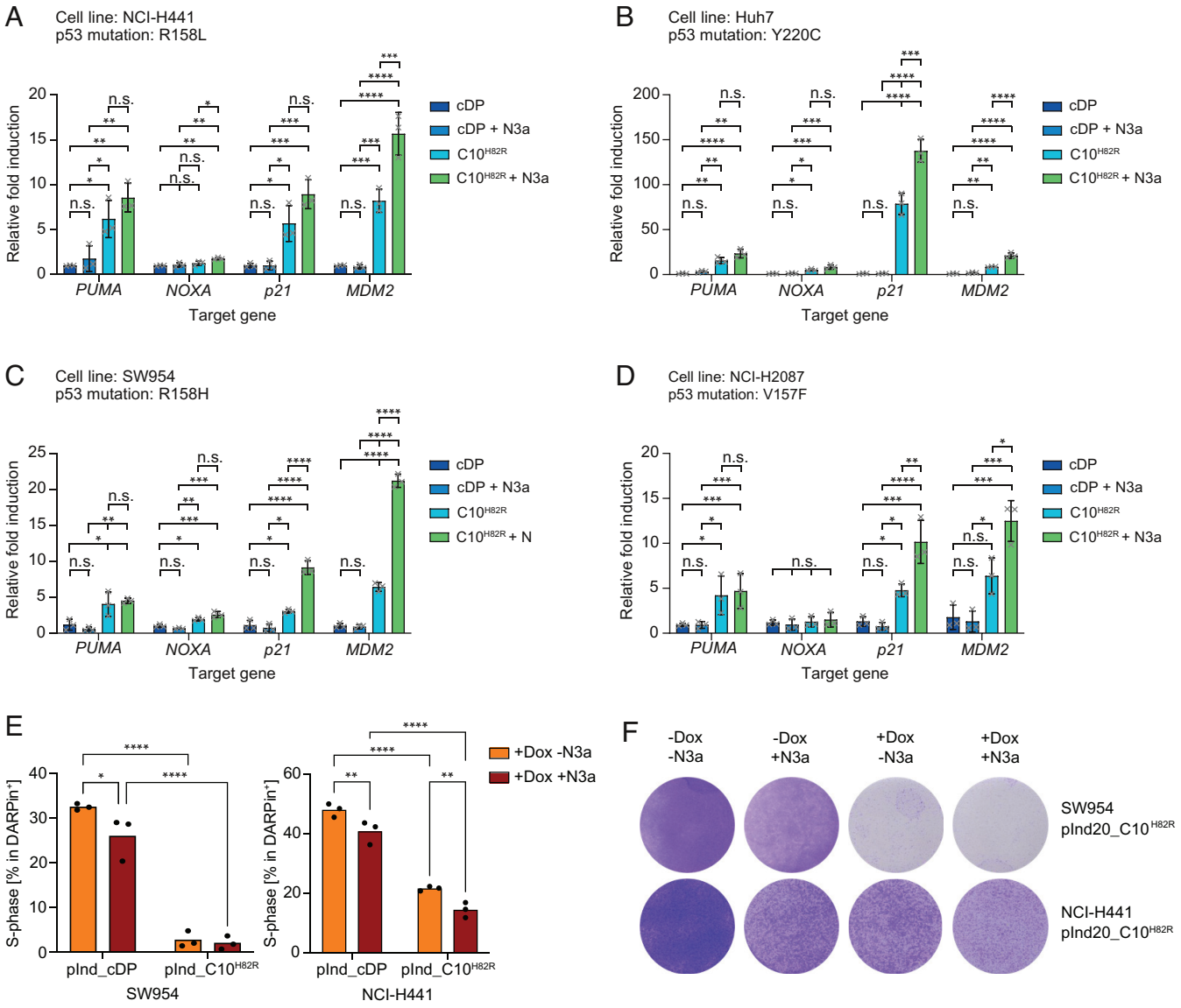

Fig. 5. DARPin-induced reactivation of p53 mutants in patient-derived cancer cell lines. (*A*) RT–qPCR analysis of the expression of p53 target genes in NCI-H441 cells harboring the p53 R158L mutation expressing either control DARPin or C10-H82R and treated with DMSO or Nutlin-3a. The total RNA was isolated from the cells and reverse transcribed into complementary DNA before analysis by qPCR. Gene expression was referenced to the housekeeping gene *HPRT-1*. (*B–D*) Same experiment as in (*A*) but with Huh7 cells harboring the p53 Y220C mutation (*B*), SW954 cells harboring the p53 R158H mutation (C), or NCI-H2087 cells harboring the p53 V157F mutation (*D*). Bar diagrams represent the mean values and the error bars the corresponding s.d. of three biological replicates. An ordinary one-way ANOVA was performed to assess the statistical significance. (*E*) Fraction of DARPin-expressing SW954 and NCI-H441 cells in S-phase, analyzed by parallel DARPin and EdU staining. Bar diagrams represent the mean of three biological replicates. Statistical significance was assessed using two-way ANOVA. (*F*) Colony formation assay showing colony growth of SW954 pInd20_C10^{H82R} (*Upper* panel) or NCI-H441 pInd20_C10^{H82R} (*Lower* panel) under Dox and N3a treatment. Dox, doxycycline; N3a, Nutlin-3a. n.s., $P > 0.05$; *$P \le 0.05$, **$P \le 0.01$, ***$P \le 0.001$, ****$P \le 0.0001$.

20 million annually and a p53 mutation rate of 50%. The 15% estimate calculated by Lu et al. (11) is likely an underestimation as it is largely based on TS mutants identified in a yeast-based screen that missed several TS mutants detectable in human cell lines. Although this was factored in to some extent, key TS hotspot mutants such as V157F or Y220C were not included. Moreover, temperature-sensitivity assays in human cell lines are typically carried out at 32 or 34 °C and, as a result, will by default fail to detect highly destabilized TS mutants.

The fact that a relatively modest threefold affinity increase—from DARPin C10 to the optimized C10-H82R variant—resulted in a substantial increase in reactivation in reporter gene assays (Fig. 3) suggests that even higher reactivation levels are achievable with potency-optimized DARPins. Such variants could, for example, be generated through directed evolution of C10 (54, 55). Also, reactivation by DARPin treatment is expected to act synergistically with therapeutic hypothermia treatment (43), which may be particularly beneficial for highly destabilized mutants. Importantly, even a small percentage of active p53 is sufficient to elicit an anti-tumor response (56). Even if DARPin treatment itself is not sufficient to induce a full apoptotic response, reactivation of p53 could resensitize tumor cells to DNA damage induced by chemotherapy. Furthermore, studies with other drugs, including CDK4/6 inhibitors and the Y220C reactivator rezatapopt, have shown that tumor regression can occur independently of apoptosis (25, 57). Instead, a prolonged cell-cycle arrest phase induced by p21 expression can lead to senescence and, via the senescence-associated secretory phenotype (SASP) pathway, to immune-mediated elimination of cancer cells.

Downloaded from https://www.pnas.org by UNIVERSITAET ZUERICH; HAUPTBIBLIOTHEK NATURWISSENSCHAFTEN on April 29, 2026 from IP address 130.60.168.8.

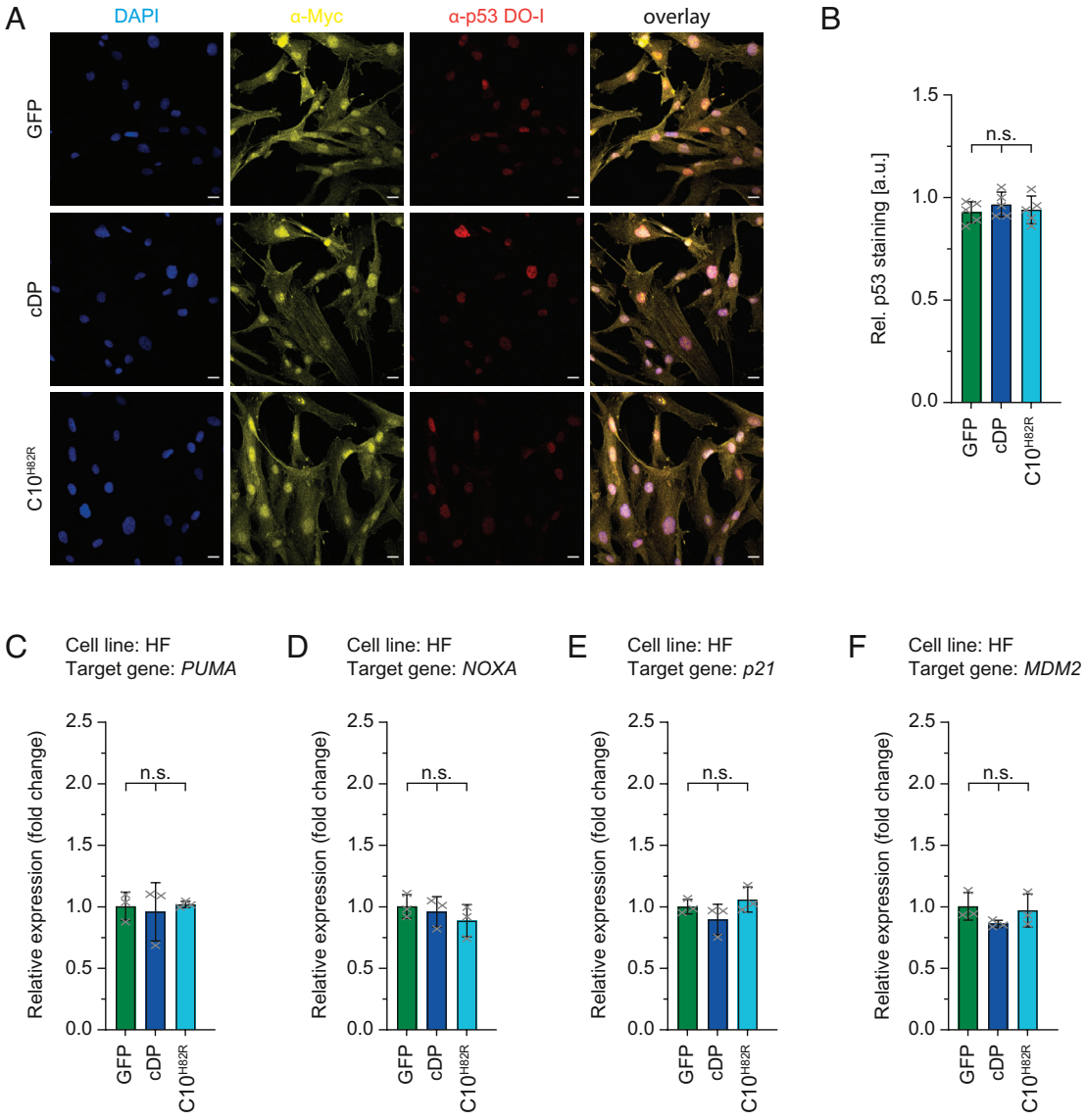

Fig. 6. Effect of DARPins on p53 activity in primary human fibroblast cells. (*A*) Immunofluorescence staining of primary human fibroblast (HF) cells transfected with mRNA encoding either the control DARPin or DARPin C10-H82R. (*B*) Quantification of the immunofluorescence staining shown in (*A*). (*C*) RT–qPCR analysis of the expression of the *PUMA* gene in primary human fibroblast cells expressing either no DARPin, control DARPin (cDP), or DARPin C10-H82R. The total RNA was isolated from the cells and reverse transcribed into complementary DNA before analysis by qPCR. Gene expression was referenced to the housekeeping gene *HPRT-1*. (*D*–*F*) The same experiment as in (*C*) but with the p53 target genes *NOXA* (D), *p21* (*E*), and *MDM2* (*F*).

A key challenge for prospective DARPin-based therapy is achieving sufficiently high intracellular protein levels in tumor cells. Viral delivery, as well as direct protein translocation, are potential strategies, and advances in mRNA/LNP-based transfection, accelerated by the SARS-CoV-2 vaccines, have opened new opportunities. The mechanism by which most LNPs based on the four-component standard formulation accumulate in the liver has been identified: LNPs become decorated with apolipoprotein E, which triggers internalization by hepatocytes expressing the corresponding receptor. This has created the possibility of modulating the tissue-specificity of LNPs by changing the lipid composition. Selective organ targeting (SORT) nanoparticles achieve organ-targeting specificity by incorporating additional lipids into the particle that alter the protein corona of serum proteins surrounding the LNPs (58). These serum proteins interact with receptors on the cell surface, making it possible to direct these particles to the lungs, spleen, or placenta (58–60). Specifically engineered LNPs can, therefore, be used to deliver therapeutic mRNAs to targeted tissues while avoiding liver accumulation. It should be pointed out, however, that the longer duration and higher levels required for therapeutic effects, compared to mRNA-based vaccination, pose a challenge (61). Therefore, in addition to tissue specificity, achieving a sufficient intracellular concentration of the DARPins is of paramount importance. Whether used to protect p53 from HPV E6-induced degradation or stabilize cancer mutants, all four DBDs of a p53 tetramer must be DARPin-bound. The intracellular levels of proteins can be boosted by stabilizing and optimizing the mRNA for example by using branched poly-A-tails (62) or circularized mRNA (63). In combination with these emerging delivery strategies, our DARPins provide an exciting opportunity for the development of potent pan-TS p53 mutant reactivators for personalized cancer therapy.

Materials and Methods

Cell Culture. NCI-H1299, NCI-H441, NCI-H2087, SW954, and Huh7 cell lines were obtained from ATCC and were cultured in RPMI 1640 supplemented with 10% FBS (Capricorn Scientific), 100 U/mL penicillin (Gibco), and 100 µg/mL

Downloaded from https://www.pnas.org by UNIVERSITAET ZUERICH; HAUPTBIBLIOTHEK NATURWISSENSCHAFTEN on April 29, 2026 from IP address 130.60.168.8.

streptomycin (Gibco) at 37 °C and 5% CO_2. Primary human fibroblasts were cultured in DMEM, supplemented with 10% FBS, 100 U/mL penicillin (Gibco), and 100 μg/mL streptomycin (Gibco) at 37 °C and 5% CO_2. Primary human fibroblasts were isolated from discarded skin obtained during surgeries. The procedure was approved by the ethics committee of the Medical Faculty of the University of Cologne (protocol no 12-088) and done according to the principles of the Declaration of Helsinki. Samples were deidentified prior to use in our study. All cell lines used in this study were frequently tested for *Mycoplasma* contaminations.

Molecular Cloning. For recombinant protein expression of DARPin C10 (see ref. 30 for the sequence) and its H82R variant as well as the wild type and mutants of the human p53 DBD (residues 94–294), a pET15b vector (Novagen, Merck KGaA) was used in *E. coli* BL21. Inserts generated by PCR were introduced into pET15b-His_{10}-TEV (N-terminal His_{10}-tag followed by a tobacco etch virus (TEV) protease cleavage site) by subcloning using BamHI and XhoI restriction sites. For transient expression in mammalian cells, PCR-generated inserts were introduced into pcDNA3.1(+) Myc (Invitrogen, Thermo Fisher Scientific) by subcloning using BamHI and XhoI restriction sites. Mutations were introduced using site-directed mutagenesis PCR with primers containing the mutated codon.

Protein Expression and Purification. DARPin C10 and p53 DBD variants were expressed and purified following published protocols (30). Further details are provided in the *SI Appendix*.

Differential Scanning Fluorimetry. Melting temperatures (T_m values) of p53 DBD variants were determined by DSF using an Agilent MX3005P real-time qPCR instrument (excitation/emission filters = 492/610 nm). Measurements were performed in a 96-well plate using an assay buffer consisting of 5 μM mutant DBD in 25 mM HEPES, pH 7.5, 500 mM NaCl, 0.5 mM TCEP, and varying concentrations (10, 20, 50, and 100 μM) of DARPin C10-H82R. The fluorescent dye SYPRO Orange (5,000×, Invitrogen) was added at a dilution of 1:1000 (total volume of 20 μL per well). The fluorescence signal was then monitored during a temperature increase from 25 to 95 °C at a heating rate of 3 °C/min, and T_m values were calculated by fitting the fluorescence curves to the Boltzmann function. DSF measurements were performed in two technical replicates, and T_m values are given as the mean ± SD.

Isothermal Titration Calorimetry. All titration experiments were performed using a MicroCal VP-ITC microcalorimeter (Malvern Instruments Ltd, UK). DARPins and p53 DBD variants were buffer-exchanged by gel filtration into ITC buffer (25 mM HEPES, pH 7.5 at 20 °C, 150 mM NaCl, 0.5 mM TCEP). The p53 DBD (5 μM) was titrated with DARPin (50 μM) in 25 injections of 10 μL each, with a spacing time of 180 s and a stirring speed of 307 rpm. Measurements were performed at 20 °C, with the reference power set to 25 μcal/s. NITPIC was used for unbiased baseline calculation and curve integration (64). Thermodynamic parameters and the final binding affinity were calculated using SEDPHAT, assuming an AB heteroassociation model (65). The first data point was excluded from the analysis.

Protein Crystallography. DARPin–p53 complexes for crystallization were prepared by mixing DARPin C10 or its second-generation variant C10-H82R and the p53 DBD at a 1:1 molar ratio in 25 mM HEPES, pH 7.5, 300 mM NaCl, 1 mM TCEP, and 5% v/v glycerol. The protein mixture was incubated at 4 °C either overnight (C10) or for 20 min (C10-H82R), and the formed protein complex was separated from unbound proteins by size-exclusion chromatography (SEC) using a Superdex 200 10/300 column with SEC buffer II (25 mM HEPES, pH 7.5, 150 mM NaCl, 0.5 mM TCEP). Central peak fractions corresponding to the protein complex were pooled and concentrated to 0.5 to 2.3 mg/mL. Crystallization was performed using the sitting-drop vapor diffusion method at 20 °C. The crystallization conditions for the various complexes are listed in *SI Appendix*, Table S1. Crystals were cryoprotected with mother liquor supplemented with 23% ethylene glycol and flash-frozen in liquid nitrogen. Diffraction data were collected at 100 K at the Swiss Light Source, Villigen, Switzerland (beamline X06SA), and the Diamond Light Source, UK (beamline I04). Data were integrated with XDS (66) and scaled with AIMLESS (67), which is part of the CCP4 package (68). The structures of the mutant p53–DARPin complexes were solved by Fourier synthesis in PHENIX (69) using the coordinates of the wild-type p53 DBD in complex with either DARPin C10 (PDB entry 8RCI) or DARPin C10-H82R (PDB entry 9FZB) as starting models, followed by initial rigid body refinement. Model building and refinement were performed using iterative cycles of manual model building in COOT (70) and refinement in PHENIX. The geometry of the final models was validated using MolProbity (71). X-ray data collection and refinement statistics are listed in *SI Appendix*, Table S2. The structural figures were prepared with PyMOL (www.pymol.org).

Transactivation Assays. For transactivation assays, H1299 cells were seeded in 24-well plates and transfected using Lipofectamine 2000 transfection reagent (Thermo Fisher Scientific) according to the manufacturer's instructions. All transfection mixes included 200 ng of pRL-CMV (Promega) for constitutive expression of *Renilla* luciferase, 200 ng of a reporter plasmid with firefly luciferase under the control of a specific promoter and a varying amount of pcDNA3.1(+) with the respective DARPin. The following two reporter constructs were used: i) pGL3 (Addgene plasmid #212936) with a p21 promoter (72) and ii) pBV-Luc BDS-2 3x WT (p53 binding site) (pBDS-2; Addgene plasmid #16515), which contains three copies of the wild-type p53-binding site from the 14-3-3σ promoter (73). pBDS-2 was a gift from Bert Vogelstein. The total amount of transfected DNA was kept constant by addition of empty pcDNA3.1(+). For each assay, an empty vector control comprising only empty pcDNA3.1(+) was transfected to determine the fold induction in the absence of DARPin. 24 h after transfection, cells were washed with PBS (Gibco), detached, and resuspended in DMEM (Gibco) into white 384-well microplates (Greiner) in quadruplicates. The assay was performed using the Dual-Glo Luciferase reporter assay kit (Promega, Cat # E2940) according to the manufacturer's instructions, and firefly as well as *Renilla* luciferase activity was measured using a Spark plate reader (Tecan). The experiment was repeated in three biological replicates, and the ratio of firefly to *Renilla* luciferase signal was normalized to the empty vector control for each biological replicate. Statistical significance was assessed by ordinary one-way ANOVA (n.s.: $P > 0.05$, *$P \leq 0.05$, **$P \leq 0.01$, ***$P \leq 0.001$, ****$P \leq 0.0001$) using Prism (Version 8.2.1, GraphPad).

Preparation of mRNA by In Vitro Transcription. For in vitro transcription, PCR-generated inserts of DARPin C10, a control DARPin, and GFP were introduced into a modified pcDNA3.1 plasmid, in which the 5′ UTR of human β-globin was inserted between the T7 promoter and the DARPin insert using NheI and HindIII. Additionally, the 3′UTR of human β-globin followed by a 120-bp poly(A) tail was cloned downstream of the DARPin insert using KpnI and SpeI. Plasmids were linearized using SpeI and in vitro transcribed using the HiScribe T7 ARCA mRNA Kit (New England Biolabs) with the modified nucleotides pseudo-UTP and 5′-methyl-CTP according to the manufacturer's instructions. RNA was purified using the RNeasy mini kit (Qiagen). RNA concentration was determined by measuring absorption at 260 nm, and RNA quality was confirmed by electrophoresis on a 1% agarose gel.

Expression of DARPins in Mutant p53 Cell Lines. HCT116 (ATCC, CCL-247) cells harboring monoallelic *TP53* mutations were generated as described in Funk et al. (46). For the generation of lentiviral plasmids for inducible expression of DARPins, the DARPin ORF was PCR-amplified using the primers 5′-CAC CAT GGA CTA CAA GGA CGA CGA CG-3′ and 5′-TTA ATT AAG CTT TTG CAG GAT TTC AGC CAG -3′ (Flag-tagged C0) or 5′-CAC CAT GGA GCA GAA GCT GAT CAG CG-3′ and 5′-TTA AGC AGC TTT CTG CAG AAC TTC AG-3′ (Myc-tagged C10) and cloned into a Gateway™ entry vector using pENTR™/D-TOPO™ Cloning Kit (Thermo Scientific, K240020SP) according to the manufacturer's protocol. DARPin ORFs were subsequently transferred into pINDUCER20 (74) plasmid using Gateway™ LR Clonase™ II Enzyme Mix (Invitrogen, 11791020) according to the manufacturer's protocol. For lentivirus production, HEK-293T cells (ATCC, CRL-3216) were transfected with lentiviral plasmids and helper plasmids pMD2.g and psPAX2 (75) using PEI transfection reagent (MedChemExpress, HY-K2014) according to the manufacturer's protocol. Supernatants containing lentivirus were collected 48 and 72 h after transfection, filtered through 0.45 μm filters (Sarstedt, 83.1826), supplemented with 8 μg/mL hexadimethrine bromide (Sigma, 107689) and used immediately for spin-infection (1 h, 1,500 rpm at 37 °C). Transduced cells were selected with 2 mg/mL neomycin (Gibco, 10131027). Expression of DARPins was induced with 500 ng/mL doxycycline (Sigma, D9891) for 48 h and maintained during the subsequent 24 h treatment with 10 μM N3a (BOC Sciences, B0084-425358) or DMSO as a solvent control. For transient transfection of DARPin mRNA, HCT116 cells were transfected using Lipofectamine MessengerMAX (Invitrogen, LMRNA015), with

Downloaded from https://www.pnas.org by UNIVERSITAET ZUERICH; HAUPTBIBLIOTHEK NATURWISSENSCHAFTEN on April 29, 2026 from IP address 130.60.168.8.

parallel treatment using 10 μM N3a (BOC Sciences, B0084-425358) or DMSO as solvent control.

Immunoblot. Cells were lysed in NP-40 Buffer (50 mM Tris-HCl, 150 mM NaCl, 5 mM EDTA, 2% NP-40, pH 8.0) supplemented with cOmplete ULTRA protease inhibitor cocktail (Roche, 4693124001) and sonicated using a Bioruptor (Diagenode) for 5 x 30 s. 20 μg protein samples were prepared using NuPAGE™ LDS Sample Buffer (Invitrogen, NP0007) and NuPAGE™ Sample Reducing Agent (Invitrogen, NP0009) and separated on NuPAGE 4 to 12% Bis-Tris polyacrylamide gels (Invitrogen, WG1402) using MOPS buffer (Invitrogen, NP0001). Following transfer to Immun-Blot PVDF Membrane (BioRad, 1620177) using NuPAGE™ Transfer Buffer (Invitrogen, NP00061), antigens were detected using the antibodies: p53 (Santa Cruz Biotechnology, sc-126; antibody DO-1; 1:1000), p21 (Santa Cruz Biotechnology, sc-6246; 1:200), and β-actin (Abcam, ab6276; 1:2500). Detection was performed using ImageLab (v6.0.1) with secondary goat anti-mouse IgG Fc HRP antibody (Invitrogen, A16084; 1:2500) and WesternBright Sirius chemiluminescent HRP conjugate (Advansta, K-12043). β-actin was detected using goat anti-mouse Alexa-488 conjugate (Invitrogen, A-11029; 1:2500). Quantification was performed using ImageJ, where band intensities were determined and normalized to the corresponding β-actin band.

Cell-Cycle Analysis. After induction of DARPin expression with 500 ng/mL doxycycline (Sigma, D9891) for 48 h, cells were treated with 10 μM N3a or DMSO as a solvent control for 24 h, with continued doxycycline treatment. For EdU incorporation, cells were incubated with 10 μM 5-ethynyl-2′-deoxyuridine (EdU; baseclick, BCN-001) for 2 h prior to fixation with 3.7% paraformaldehyde (PFA) in PBS (pH 7.4) for 15 min at RT. Following fixation, cells were washed once with PBS and once with blocking buffer (2% BSA in PBS), then permeabilized with 0.1% Triton X-100 in PBS for 20 min at RT. The EdU Click-iT reaction was performed by incubating cells for 30 min at RT in the dark in 250 μL Click-iT reaction mix (4 mM $CuSO_4$, 1 μM Eterneon-Red 645 Azide (baseclick, BCFA-201), 100 mM ascorbic acid in PBS). After the reaction, cells were washed once with blocking buffer and once with 0.1 M glycine in PBS, followed by blocking in blocking buffer for 10 min at RT. DARPin staining was performed using the following primary antibodies: anti-FLAG (Cell Signaling, #2276, clone 9B11; 1:50) for the control DARPin and anti-myc (Sigma-Aldrich, F1804; 1:50) for DARPin C10. Incubations were carried out for 1 h at 37 °C, 300 rpm. Cells were washed twice with blocking buffer and subsequently incubated with the secondary antibody goat anti-mouse Alexa-488 conjugate (Invitrogen, A-11029; 1:50) for 1 h at 37 °C, 300 rpm. Cells were washed twice in blocking buffer and analyzed on a CytoFLEX LX cytometer (Beckman Coulter).

Colony Formation Assay. 2×10^5 cells were seeded per 6 cm plate (Sarstedt, 83.3901). After 24 h, cells were treated with 500 ng/mL doxycycline (Sigma, D9891) and 10 μM N3a (BOC Sciences, B0084-425358) or DMSO as the solvent control. Treatments were refreshed every 2 d until control plates reached confluence. Plates were then fixed with 70% ethanol for 30 min at RT and stained for 15 min with 0.2% crystal violet in 10% ethanol (Sigma-Aldrich, HT90132). Plates were scanned using Epson Scan (v3.24G), and images were processed with Adobe Photoshop CS6 (v13.0.1). For quantification, the stain was eluted with 20% acetic acid, and absorbance was measured at 590 nm using a CYTATION 3 imaging plate reader with Gen5 software (v3.08).

Quantitative PCR (qPCR). For qPCR analysis of the expression of p53 target genes, NCI-H441, NCI-H2087, SW954, Huh7, or primary human fibroblast cells were transfected with mRNA encoding the respective DARPin using Lipofectamine MessengerMAX transfection reagent (Thermo Fisher Scientific) according to the manufacturer's instructions. 24 h after transfection, cells were washed with PBS, detached, and mRNA was isolated using the RNeasy mini kit (Qiagen). Reverse transcription of mRNA was performed using the SuperScript™ IV VILO™ mastermix with ezDNase™-enzyme kit (Thermo Fisher Scientific). Both kits were used according to the manufacturer's instructions. Quantitative PCR was performed in technical triplicates using the TaqMan fast advanced Master Mix and the respective TaqMan Assay (Thermo Fisher Scientific) on a QuantStudio 5 Real Time PCR system (Thermo Fisher Scientific). Target gene expression was normalized to the housekeeping gene HPRT-1. The experiment was repeated in three biological replicates, and statistical significance was assessed by ordinary one-way ANOVA (n.s.: $P > 0.05$, *$P \leq 0.05$, **$P \leq 0.01$, ***$P \leq 0.001$, ****$P \leq 0.0001$) using Prism (Version 8.2.1, GraphPad)

Caspase Glo 3/7 Assay. NCI-H441, NCI-H2087, SW954, or Huh7 cells were transfected with mRNA encoding the respective DARPin using Lipofectamine MessengerMAX transfection reagent (Thermo Fisher Scientific) according to the manufacturer's instructions. 24 h after transfection, cells were washed with PBS and the Caspase Glo Assay was performed using the Caspase Glo 3/7 Assay kit (Promega, Cat # G8090) according to the manufacturer's instructions.

Data, Materials, and Software Availability. The coordinates and structure factors of the p53 mutant DBDs in complex with DARPin C10 or DARPin C10-H82R have been deposited in the Protein Data Bank (PDB) under the following accession numbers: 9SPM (76) (V143A mutant), 9SPN (77) (V157F mutant), 9SPO (78) (Y220C mutant), 9SPP (79) (Y234C mutant), 9SPQ (80) (V272M mutant), 9SPR (81) (R282W mutant), and 9SPS (82) (E285K mutant).

ACKNOWLEDGMENTS. The research was funded by the DFG (DO 545/24-1), the Centre for Biomolecular Magnetic Resonance (BMRZ), the Clusterproject ENABLE (funded by the Hessian Ministry for Science and the Arts), and the BMBF (PROXIDRUGS) to V.D. A.C.J. received funding from the German Research Foundation (DFG) grant JO 1473/1-3. A.C.J. and V.D. are also grateful for funding from the Wilhelm-Sander-Stiftung (2025.152.1). S.K. and A.C.J. acknowledge support from the German Cancer Aid grant TACTIC (70115201), which is part of the preclinical cancer drug development network (preCDD). D.M. is supported by an Onassis Foundation fellowship (Scholarship ID: F ZU 049-1/ 2024-2025). D.M., D.-I.B., S.K., and A.C.J. are grateful for support by the Structural Genomics Consortium (SGC), a registered charity (No:1097737) that received funds from Bayer AG, Boehringer Ingelheim, Bristol Myers Squibb, Genentech, Genome Canada through Ontario Genomics Institute, [OGI-196], EU/EFPIA/OICR/McGill/KTH/Diamond Innovative Medicines Initiative 2 Joint Undertaking [EUbOPEN grant 875510], Janssen, Merck KGaA, Pfizer, and Takeda. T.S. is funded by the DFG (GRK2573, STI 182/13-1, STI 182/15-1, and STI 182/19-1), Deutsche Krebshilfe (70116475), Wilhelm-Sander-Stiftung (2022.129.1 and 2025.201.1), Bundesministerium für Bildung und Forschung (German Center for Lung Research - DZL), and Hessisches Ministerium für Wissenschaft und Kunst (LOEWE iCANx). B.A. was funded by the DFG (AK 42/12-1). We thank the staff at beamline X06SA of the Swiss Light Source and beamline I04 of the Diamond Light Source for assistance during data collection. Portions of the paper were developed from the PhD thesis of P.M.

Author affiliations: [a]Institute of Biophysical Chemistry and Center for Biomolecular Magnetic Resonance, Goethe University, Frankfurt 60438, Germany; [b]Institute of Pharmaceutical Chemistry, Goethe University, Frankfurt 60438, Germany; [c]Structural Genomics Consortium, Buchmann Institute for Molecular Life Sciences, Goethe University, Frankfurt 60438, Germany; [d]Institute of Molecular Oncology, Universities of Giessen and Marburg Lung Center, Member of the German Center for Lung Research, Philipps-University, Marburg 35043, Germany; [e]International Max Planck Research School on Cellular Biophysics, Frankfurt 60438, Germany; [f]Department of Biochemistry, University of Zurich, Zurich 8057, Switzerland; [g]Institute of Virology, Medical Faculty and University Hospital Cologne, University of Cologne, Cologne 50935, Germany; [h]Genomics Core Facility, Philipps-University, Marburg 35043, Germany; and [i]Institute for Lung Health, Justus Liebig University, Giessen 35392, Germany

Author contributions: P.M., D.-I.B., T.S., A.C.J., and V.D. designed research; P.M., D.-I.B., J.S.F., B.Y., D.M., J.H., B.S., and T.T. performed research; B.D., J.V.S., and A.P. contributed new reagents/analytic tools; P.M., D.-I.B., J.S.F., B.Y., D.M., J.H., B.D., J.V.S., S.K., B.A., A.P., T.S., and A.C.J. analyzed data; and A.C.J. and V.D. wrote the paper.

1. A. C. Joerger, A. R. Fersht, The p53 pathway: Origins, inactivation in cancer, and emerging therapeutic approaches. *Annu. Rev. Biochem.* **85**, 375–404 (2016).
2. K. H. Khoo, C. S. Verma, D. P. Lane, Drugging the p53 pathway: Understanding the route to clinical efficacy. *Nat. Rev. Drug Discov.* **13**, 217–236 (2014).
3. O. Hassin, M. Oren, Drugging p53 in cancer: One protein, many targets. *Nat. Rev. Drug Discov.* **22**, 127–144 (2023).
4. A. C. Joerger, T. Stiewe, T. Soussi, TP53: The unluckiest of genes? *Cell Death Differ.* **32**, 219–224 (2025).
5. A. C. Joerger, A. R. Fersht, Structure-function-rescue: The diverse nature of common p53 cancer mutants. *Oncogene* **26**, 2226–2242 (2007).
6. P. Hainaut, G. P. Pfeifer, Somatic TP53 mutations in the era of genome sequencing. *Cold Spring Harb. Perspect. Med.* **6**, a026179 (2016).
7. T. Stiewe, T. E. Haran, How mutations shape p53 interactions with the genome to promote tumorigenesis and drug resistance. *Drug Resist. Updat.* **38**, 27–43 (2018).
8. A. N. Bullock, J. Henckel, A. R. Fersht, Quantitative analysis of residual folding and DNA binding in mutant p53 core domain: Definition of mutant states for rescue in cancer therapy. *Oncogene* **19**, 1245–1256 (2000).

Downloaded from https://www.pnas.org by UNIVERSITAET ZUERICH; HAUPTBIBLIOTHEK NATURWISSENSCHAFTEN on April 29, 2026 from IP address 130.60.168.8.

9. G. Wang, A. R. Fersht, Multisite aggregation of p53 and implications for drug rescue. *Proc. Natl. Acad. Sci. U.S.A.* **114**, E2634–E2643 (2017).
10. L. R. Dearth *et al.*, Inactive full-length p53 mutants lacking dominant wild-type p53 inhibition highlight loss of heterozygosity as an important aspect of p53 status in human cancers. *Carcinogenesis* **28**, 289–298 (2007).
11. J. Lu, L. Chen, Z. Song, M. Das, J. Chen, Hypothermia effectively treats tumors with temperature-sensitive p53 mutations. *Cancer Res.* **81**, 3905–3915 (2021).
12. C. J. Di Como, C. Prives, Human tumor-derived p53 proteins exhibit binding site selectivity and temperature sensitivity for transactivation in a yeast-based assay. *Oncogene* **16**, 2527–2539 (1998).
13. A. N. Bullock, A. R. Fersht, Rescuing the function of mutant p53. *Nat. Rev. Cancer* **1**, 68–76 (2001).
14. A. C. Joerger, H. C. Ang, A. R. Fersht, Structural basis for understanding oncogenic p53 mutations and designing rescue drugs. *Proc. Natl. Acad. Sci. U.S.A.* **103**, 15056–15061 (2006).
15. A. C. Joerger *et al.*, Exploiting transient protein states for the design of small-molecule stabilizers of mutant p53. *Structure* **23**, 2246–2255 (2015).
16. M. R. Bauer *et al.*, Targeting cavity-creating p53 cancer mutations with small-molecule stabilizers: The Y220X paradigm. *ACS Chem. Biol.* **15**, 657–668 (2020).
17. F. M. Boeckler *et al.*, Targeted rescue of a destabilized mutant of p53 by an in silico screened drug. *Proc. Natl. Acad. Sci. U.S.A.* **105**, 10360–10365 (2008).
18. R. Wilcken *et al.*, Halogen-enriched fragment libraries as leads for drug rescue of mutant p53. *J. Am. Chem. Soc.* **134**, 6810–6818 (2012).
19. X. Liu *et al.*, Small molecule induced reactivation of mutant p53 in cancer cells. *Nucleic Acids Res.* **41**, 6034–6044 (2013).
20. M. G. J. Baud *et al.*, Aminobenzothiazole derivatives stabilize the thermolabile p53 cancer mutant Y220C and show anticancer activity in p53-Y220C cell lines. *Eur. J. Med. Chem.* **152**, 101–114 (2018).
21. J. R. Stephenson Clarke *et al.*, Discovery of nanomolar-affinity pharmacological chaperones stabilizing the oncogenic p53 mutant Y220C. *ACS Pharmacol. Transl. Sci.* **5**, 1169–1180 (2022).
22. T. Klett *et al.*, Covalent fragments acting as tyrosine mimics for mutant p53–Y220C rescue by nucleophilic aromatic substitution. *ACS Pharmacol. Transl. Sci.* **7**, 3984–3999 (2024).
23. M. R. Bauer *et al.*, A structure-guided molecular chaperone approach for restoring the transcriptional activity of the p53 cancer mutant Y220C. *Future Med. Chem.* **11**, 2491–2504 (2019).
24. K. Z. Guiley, K. M. Shokat, A small molecule reacts with the p53 somatic mutant Y220C to rescue wild-type thermal stability. *Cancer Discov.* **13**, 56–69 (2023).
25. A. M. Puzio-Kuter *et al.*, Restoration of the tumor suppressor function of Y220C-mutant p53 by Rezatapopt, a small-molecule reactivator. *Cancer Discov.* **15**, 1159–1179 (2025).
26. E. E. Dumbrava *et al.*, Phase 1 study of Rezatapopt, a p53 reactivator, in TP53 Y220C-mutated tumors. *N. Engl. J. Med.* **394**, 872–883 (2026).
27. S. Chen *et al.*, Arsenic trioxide rescues structural p53 mutations through a cryptic allosteric site. *Cancer Cell* **39**, 225–239 (2021).
28. H. Song *et al.*, Diverse rescue potencies of p53 mutations to ATO are predetermined by intrinsic mutational properties. *Sci. Transl. Med.* **15**, eabn9155 (2023).
29. Y. Tang *et al.*, Repurposing antiparasitic antimonials to noncovalently rescue temperature-sensitive p53 mutations. *Cell Rep.* **39**, 110622 (2022).
30. P. Münick *et al.*, DARPin-induced reactivation of p53 in HPV-positive cells. *Nat. Struct. Mol. Biol.* **32**, 790–801 (2025).
31. M. Scheffner, B. A. Werness, J. M. Huibregtse, A. J. Levine, P. M. Howley, The E6 oncoprotein encoded by human papillomavirus types 16 and 18 promotes the degradation of p53. *Cell* **63**, 1129–1136 (1990).
32. M. Hufbauer, B. Akgul, Molecular mechanisms of human papillomavirus induced skin carcinogenesis. *Viruses* **9**, 187 (2017).
33. D. Martinez-Zapien *et al.*, Structure of the E6/E6AP/p53 complex required for HPV-mediated degradation of p53. *Nature* **529**, 541–545 (2016).
34. Y. L. Boersma, A. Plückthun, DARPins and other repeat protein scaffolds: Advances in engineering and applications. *Curr. Opin. Biotechnol.* **22**, 849–857 (2011).
35. A. Plückthun, Designed ankyrin repeat proteins (DARPins): Binding proteins for research, diagnostics, and therapy. *Annu. Rev. Pharmacol. Toxicol.* **55**, 489–511 (2015).
36. A. Strubel *et al.*, Designed ankyrin repeat proteins as a tool box for analyzing p63. *Cell Death Differ.* **29**, 2445–2458 (2022).
37. A. Strubel *et al.*, DARPins detect the formation of hetero-tetramers of p63 and p73 in epithelial tissues and in squamous cell carcinoma. *Cell Death Dis.* **14**, 674 (2023).
38. P. Münick *et al.*, DARPins as a novel tool to detect and degrade p73. *Cell Death Dis.* **15**, 909 (2024).
39. B. D. Wallentine *et al.*, Structures of oncogenic, suppressor and rescued p53 core-domain variants: Mechanisms of mutant p53 rescue. *Acta Crystallogr. Section D-Struct. Biol.* **69**, 2146–2156 (2013).
40. D. I. Balourdas, A. M. Markl, A. Kramer, G. Settanni, A. C. Joerger, Structural basis of p53 inactivation by cavity-creating cancer mutations and its implications for the development of mutant p53 reactivators. *Cell Death Dis.* **15**, 408 (2024).
41. K. C. de Andrade *et al.*, The TP53 database: Transition from the International Agency for Research on Cancer to the US National Cancer Institute. *Cell Death Differ.* **29**, 1071–1073 (2022).
42. B. Leroy *et al.*, The TP53 website: An integrative resource centre for the TP53 mutation database and TP53 mutant analysis. *Nucleic Acids Res.* **41**, D962–D969 (2013).
43. J. Lu, L. Chen, Z. Fatima, J. Huang, J. Chen, Synergistic rescue of temperature-sensitive p53 mutants by hypothermia and arsenic trioxide. *Mol. Carcinog.* **63**, 2205–2217 (2024).
44. D. Grochova *et al.*, Analysis of transactivation capability and conformation of p53 temperature-dependent mutants and their reactivation by amifostine in yeast. *Oncogene* **27**, 1243–1252 (2008).
45. K. Shiraishi *et al.*, Isolation of temperature-sensitive p53 mutations from a comprehensive missense mutation library. *J. Biol. Chem.* **279**, 348–355 (2004).
46. J. S. Funk *et al.*, Deep CRISPR mutagenesis characterizes the functional diversity of TP53 mutations. *Nat. Genet.* **57**, 140–153 (2025).
47. F. Ponchel, J. Milner, Temperature sensitivity of human wild-type and mutant p53 proteins expressed in vivo. *Br. J. Cancer* **77**, 1555–1561 (1998).
48. Y. Haupt, R. Maya, A. Kazaz, M. Oren, Mdm2 promotes the rapid degradation of p53. *Nature* **387**, 296–299 (1997).
49. L. T. Vassilev *et al.*, In vivo activation of the p53 pathway by small-molecule antagonists of MDM2. *Science* **303**, 844–848 (2004).
50. S. B. Stanfill *et al.*, From cultivation to cancer: Formation of N-nitrosamines and other carcinogens in smokeless tobacco and their mutagenic implications. *Crit. Rev. Toxicol.* **53**, 658–701 (2023).
51. J. A. Barta, K. Pauley, A. V. Kossenkov, S. B. McMahon, The lung-enriched p53 mutants V157F and R158L/P regulate a gain of function transcriptome in lung cancer. *Carcinogenesis* **41**, 67–77 (2020).
52. T. M. Hernandez-Boussard, P. Hainaut, A specific spectrum of p53 mutations in lung cancer from smokers: Review of mutations compiled in the IARC p53 database. *Environ. Health Perspect.* **106**, 385–391 (1998).
53. D. Mavridi *et al.*, Targeting the p53 cancer mutants Y220C, Y220N, and Y220S with the small-molecule stabilizer rezatapopt. *Cell Death Dis.* **17**, 268 (2026).
54. C. Zahnd, C. A. Sarkar, A. Plückthun, Computational analysis of off-rate selection experiments to optimize affinity maturation by directed evolution. *Protein Eng. Des. Sel.* **23**, 175–184 (2010).
55. C. Zahnd *et al.*, A designed ankyrin repeat protein evolved to picomolar affinity to Her2. *J. Mol. Biol.* **369**, 1015–1028 (2007).
56. B. Klimovich *et al.*, Partial p53 reactivation is sufficient to induce cancer regression. *J. Exp. Clin. Cancer Res.* **41**, 80 (2022).
57. R. Kudo *et al.*, Long-term breast cancer response to CDK4/6 inhibition defined by TP53-mediated geroconversion. *Cancer Cell* **42**, 1983 (2024).
58. S. A. Dilliard, Q. Cheng, D. J. Siegwart, On the mechanism of tissue-specific mRNA delivery by selective organ targeting nanoparticles. *Proc. Natl. Acad. Sci. U.S.A.* **118**, e2109256118 (2021).
59. K. L. Swingle *et al.*, Placenta-tropic VEGF mRNA lipid nanoparticles ameliorate murine pre-eclampsia. *Nature* **637**, 412–421 (2025).
60. Y. Sun *et al.*, In vivo editing of lung stem cells for durable gene correction in mice. *Science* **384**, 1196–1202 (2024).
61. E. Rohner, R. Yang, K. S. Foo, A. Goedel, K. R. Chien, Unlocking the promise of mRNA therapeutics. *Nat. Biotechnol.* **40**, 1586–1600 (2022).
62. H. Chen *et al.*, Branched chemically modified poly(A) tails enhance the translation capacity of mRNA. *Nat. Biotechnol.* **43**, 194–203 (2024), 10.1038/s41587-024-02174-7.
63. R. Chen *et al.*, Engineering circular RNA for enhanced protein production. *Nat. Biotechnol.* **41**, 262–272 (2023).
64. S. Keller *et al.*, High-precision isothermal titration calorimetry with automated peak-shape analysis. *Anal. Chem.* **84**, 5066–5073 (2012).
65. J. C. D. Houtman *et al.*, Studying multisite binary and ternary protein interactions by global analysis of isothermal titration calorimetry data in SEDPHAT: Application to adaptor protein complexes in cell signaling. *Protein Sci.* **16**, 30–42 (2007).
66. W. Kabsch, Xds. *Acta Crystallogr. D Biol. Crystallogr.* **66**, 125–132 (2010).
67. P. R. Evans, An introduction to data reduction: Space-group determination, scaling and intensity statistics. *Acta Crystallogr. D* **67**, 282–292 (2011).
68. M. D. Winn *et al.*, Overview of the CCP4 suite and current developments. *Acta Crystallogr. D Biol. Crystallogr.* **67**, 235–242 (2011).
69. D. Liebschner *et al.*, Macromolecular structure determination using X-rays, neutrons and electrons: Recent developments in Phenix. *Acta Crystallogr. D. Struct. Biol.* **75**, 861–877 (2019).
70. P. Emsley, B. Lohkamp, W. G. Scott, K. Cowtan, Features and development of coot. *Acta Crystallogr. D* **66**, 486–501 (2010).
71. C. J. Williams *et al.*, Molprobity: More and better reference data for improved all-atom structure validation. *Protein Sci.* **27**, 293–315 (2018).
72. A. Brdar *et al.*, p53 isoforms have a high aggregation propensity, interact with chaperones and lack binding to p53 interaction partners. *Elife* **13**, RP103537 (2025).
73. H. Hermeking *et al.*, 14-3-3 sigma is a p53-regulated inhibitor of G2/M progression. *Mol. Cell* **1**, 3–11 (1997).
74. K. L. Meerbrey *et al.*, The pINDUCER lentiviral toolkit for inducible RNA interference in vitro and in vivo. *Proc. Natl. Acad. Sci. U.S.A.* **108**, 3665–3670 (2011).
75. M. Wiznerowicz, D. Trono, Conditional suppression of cellular genes: Lentivirus vector-mediated drug-inducible RNA interference. *J. Virol.* **77**, 8957–8961 (2003).
76. D. I. Balourdas, P. Münick, S. Knapp, V. Dötsch, A. C. Joerger, p53 cancer mutant V143A in complex with DARPin C10. Protein Data Bank. https://doi.org/10.2210/pdb9SPM/pdb. Deposited 17 September 2025.
77. D. I. Balourdas, P. Münick, S. Knapp, V. Dötsch, A. C. Joerger, p53 cancer mutant V157F in complex with DARPin C10. Protein Data Bank. https://doi.org/10.2210/pdb9SPN/pdb. Deposited 17 September 2025.
78. D. I. Balourdas, P. Münick, S. Knapp, V. Dötsch, A. C. Joerger, p53 cancer mutant Y220C in complex with DARPin C10. Protein Data Bank. https://doi.org/10.2210/pdb9SPO/pdb. Deposited 17 September 2025.
79. D. I. Balourdas, P. Münick, S. Knapp, V. Dötsch, A. C. Joerger, p53 cancer mutant Y234C in complex with DARPin C10. Protein Data Bank. https://doi.org/10.2210/pdb9SPP/pdb. Deposited 17 September 2025.
80. D. I. Balourdas, P. Münick, S. Knapp, V. Dötsch, A. C. Joerger, p53 cancer mutant V272M in complex with DARPin C10. Protein Data Bank. https://doi.org/10.2210/pdb9SPQ/pdb. Deposited 17 September 2025.
81. D. I. Balourdas, P. Münick, S. Knapp, V. Dötsch, A. C. Joerger, p53 cancer mutant R282W in complex with DARPin C10. Protein Data Bank. https://doi.org/10.2210/pdb9SPR/pdb. Deposited 17 September 2025.
82. D. Mavridi, B. Yüksel, S. Knapp, V. Dötsch, A. C. Joerger, p53 cancer mutant E285K in complex with DARPin C10-H82R. Protein Data Bank. https://doi.org/10.2210/pdb9SPS/pdb. Deposited 17 September 2025.

Downloaded from https://www.pnas.org by UNIVERSITAET ZUERICH; HAUPTBIBLIOTHEK NATURWISSENSCHAFTEN on April 29, 2026 from IP address 130.60.168.8.